mathematics

MDPI

Article

Third-Order Superharmonic Resonance Analysis and Control in a Nonlinear Dynamical System

Ali Kandil [1,2,*], Yasser S. Hamed [3], Mohamed S. Mohamed [3], Jan Awrejcewicz [4] and Maksymilian Bednarek [4]

1 Department of Mathematics, Institute of Basic and Applied Sciences, Egypt-Japan University of Science and Technology (E-JUST), New Borg El-Arab City 21934, Egypt
2 Department of Physics and Engineering Mathematics, Faculty of Electronic Engineering, Menoufia University, Menouf 32952, Egypt
3 Department of Mathematics and Statistics, College of Science, Taif University, P.O. Box 11099, Taif 21944, Saudi Arabia; yasersalah@tu.edu.sa (Y.S.H.); m.saaad@tu.edu.sa (M.S.M.)
4 Department of Automation, Biomechanics and Mechatronics, Faculty of Mechanical Engineering, Lodz University of Technology, 90-924 Lodz, Poland; jan.awrejcewicz@p.lodz.pl (J.A.); maksymilian.bednarek@p.lodz.pl (M.B.)
* Correspondence: ali.kandil@ejust.edu.eg or alikandil21@el-eng.menofia.edu.eg or alikandil21@yahoo.com

Abstract: The present work discusses the dynamical analysis of the superharmonic resonance in a mass-damper-spring model controlled by a cubic-position negative-velocity feedback (CPNV) controller. Thanks to the harmonic balance technique, the approximate solution of the studied model can be extracted and then checked for stability using Floquet exponents. The cubic-position control gain is adjusted in order to suppress the model's steady oscillations. In addition, the negative-velocity control gain is adjusted in order to shrink the period of the transient oscillations. Several plots are included to relate the car's oscillatory amplitude with the model's different parameters pre- and post-control so that we can determine the optimum conditions for running the model safely.

Keywords: superharmonic resonance; cubic-position negative-velocity feedback controller; mass-damper-spring model; harmonic balance method; Floquet exponents

MSC: 34C15; 34C23; 34C25; 34C60; 34F15; 37C75; 37N35; 70J25; 70J35; 70K30; 70K40; 70K42; 93B52; 93D15

Citation: Kandil, A.; Hamed, Y.S.; Mohamed, M.S.; Awrejcewicz, J.; Bednarek, M. Third-Order Superharmonic Resonance Analysis and Control in a Nonlinear Dynamical System. *Mathematics* **2022**, *10*, 1282. https://doi.org/10.3390/math10081282

Academic Editor: Ioannis G. Stratis

Received: 10 March 2022
Accepted: 11 April 2022
Published: 12 April 2022

1. Introduction

In nonlinear dynamical systems, the secondary resonance is a case that should be considered if the system is hardly excited. In other words, when the excitation frequency is away from the system's linear natural frequency, the effect of the excitation will be small unless its amplitude is large. One of the cases of interest is when the excitation force oscillates with a frequency about one-third of the system's linear natural frequency. Such a case is called a third-order superharmonic resonance case, which is our case of study in this research. Many researchers all over the world have analyzed, theoretically and experimentally, the nonlinear dynamics of the models excited by the third-order superharmonic resonance. Rahman and Burton [1] proposed a second-order perturbation analysis of the third-order superharmonic resonance in a Duffing oscillator in order to obtain realistic steady-state stability results. They concluded that the derived second-order approximate solution of the studied problem was necessary to explore the double-jump phenomenon in a harmonically excited single degree of freedom (SDOF) oscillator. Nayfeh and Sanchez [2] investigated the response of a softening-type damped Duffing oscillator subjected to a harmonic excitation in a frequency–amplitude space. They predicted, through the analysis, the symmetry breaking, period doubling, and jumps in either bounded or unbounded waveforms. Benedettini and Rega [3] studied the planar nonlinear oscillations of elastic cables excited by second- and third-order superharmonic resonance. They pictured the interactions between the main studied superharmonic components and verified them by numerical simulations. Burton and Anderson [4] presented the results of a nonlinear dynamical system's response subjected to chaotic input where the response spectra for the system was included, in which the damping and excitation frequency parameters were fixed. They concluded that the proposed randomness of the cascaded oscillator responses $u_n(t)$ became quicker when increasing n for small n. However, these responses reached a specific limit for large n, at which the excitation and response had identical statistical aspects. Rahman and Burton [5] applied the multiple time scales with high-order approximations in order to extract the steady-state responses of a weakly nonlinear, harmonically forced oscillator. They adopted two different approaches of the studied method that led to two different results regarding the frequency-response curves bending and their maxima. Sanchez and Nayfeh [6] used a Floquet theory algorithm to determine the instability regions of a damped, softening-type Duffing oscillator subjected to a parametric excitation. They predicted the instabilities locus of the approximate solutions in the frequency-response curves in order to understand the overall dynamical behavior of the studied model. Rega et al. [7] studied, in detail, the chaotic dynamics of a harmonically excited SDOF asymmetric dynamical system whose nonlinear dynamics were continuum with the help of computer simulations. Their studied model exhibited a single equilibrium position once they included quadratic–cubic nonlinearities and geometrical–mechanical aspects in the equation of motion. Gottlieb and Yim [8] explained a taut multi-point mooring system including large geometric nonlinearity with wave and current excitation. They applied a semi-analytical method that evinced the local instabilities and bifurcations leading to a chaotic behavior. Hamdan and Burton [9] showed the qualitative nature of the harmonic balance (HB) solution of a softening-type Duffing oscillator as well as its local stability. They showed qualitatively how the HB solution changed the in case of using two harmonic instead of one only along with the effect on its local stability analysis. Hassan [10] investigated, analytically and numerically, the third-order superharmonic resonance in two different types of an excited Duffing oscillator. It was concluded that a sudden transition into chaos could be caused by a saddle-node bifurcation for the third-order superharmonic resonance case. Addison [11] introduced two models of nonlinear Duffing oscillators: one of them was chaotically excited, and the other one was elastically coupled. The author characterized the chaotic behavior of the two systems, applying the Grassberger-Procaccia algorithm in order to determine the growth or decay of oscillations number. Adrezin et al. [12] introduced a survey on offshore-compliant structures in order to explore the modeling approaches applied by workers for a better understanding of these structures behavior. They focused on the static and dynamic behaviors of the studied structures subjected to wind, waves, and current where there were similarities in the structural and environmental complexities. Lukomsky and Bobkov [13] presented a spectral technique to build an asymptotic expansion describing the periodic responses in conservative and self-excited weakly nonlinear dynamical systems. They proved the validity of the proposed asymptotic expansion in the periodic motion's domain of definite type until reaching the separatrix. Vaidya and He [14] proposed a theoretical explanation of the observed Trans-Spectral Coherence for the generated signal from a chaotic Duffing oscillator. They expected a strong coherence in case that the Duffing oscillator exhibited periodic motions, while there was no phase coherence in case of chaotic motions. Luongo and Paolone [15] applied the multiple time scales method of higher orders in order to extract the approximate solutions of general multi-parameter, nonlinear mechanical systems. They derived the perturbation equations involving the control and imperfection parameters in order to compare among four different approaches of the method adopted. Al-Qaisia and Hamdan [16] were concerned with the steady-state response of the same period of the excitation force in a strongly nonlinear oscillator. They utilized one-harmonic and two-harmonic HB approximations in order to predict the qualitative behavior of the oscillator's actual solution. Khanin et al. [17] generalized a computer implementation of the multiple time scales technique and its application to nonlinear vibration problems. They discussed, using MATHEMATICA, the formulation of the macro-steps used for developing the computational system for multi degree of freedom (MDOF) dynamical systems. Hamdan et al. [18] presented second-order approximate solutions of the steady-state principal parametric resonance response of a vertically-mounted flexible cantilever beam subjected to a vertical harmonic base motion. They adopted two versions of multiple-scales method, where one of them led to more accurate second-order approximations, while the two-term HB solutions improved the accuracy of approximations. Nielsen and Kirkegaard [19] analyzed the cables in stayed bridges and TV towers excited by a harmonically varying in-plane motion of the upper support point. They applied the averaging method with the superharmonic response in order to explore a substantial combinatorial harmonic component accompanied with a circular frequency. Cartmell et al. [20] addressed the mathematical basics of the multiple time-scales perturbation technique used with weakly nonlinear mechanical systems that were defined by ordinary differential equations. The authors discussed the strengths, the adaptability, and the weaknesses of the studied method in order to make a survey about modeling accuracy of different dynamical systems. Rega [21] presented a review on modelling the cables and other mechanical system through the continuum equations and their discretized form of analysis. The author reported, based on measurements and diagnosis, the chaotic response as well as the global bifurcations of different cable models. Berlioz and Lamarque [22] investigated, theoretically and experimentally, an inclined cable subjected to the boundary motion condition where its nonlinear behavior was predicted. They modelled the cable with both SDOF and 2DOF systems for the in-plane deflections and carried out experimental work on the mechanical model for validation purpose. Wang et al. [23] studied a nonlinear vibration isolation system whose response was chaotic, and its line spectrum was reduced. They applied the HB method in order to explore different harmonics interactions where the fundamental harmonic's energy could be channeled to other harmonics. Kovacic et al. [24] studied an asymmetric Duffing oscillator with hardening characteristics and its linear stiffness term absent in case of primary resonance. They adopted the HB method to extract the model's approximate solution where different frequency-response curves with multi-valued solutions were explored. Macdonald et al. [25] built their analysis on multi-mode cables with support harmonic excitation frequency near any mode's natural frequency. They concluded that the excited mode could affect the boundaries of stability of the other unexcited modes in comparison with the previous solutions approached. Dankowicz and Lacarbonara [26] obtained higher-order approximations with the help of multiple time-scales method in order to study the oscillatory response of a nonlinear dynamical system. They concluded that the relation between the oscillation frequency and measured quantities was unique and not influenced by any other conditions. Vassilopoulou and Gantes [27] investigated the nonlinear dynamics of a simple cable net consisting of dual crossing cables in perpendicular vertical planes, having the same span and opposite sags. They simplified the problem for showing the nonlinear phenomena, i.e., the curve's bending, the jump phenomena, and instability boundaries due to superharmonic and subharmonic resonances. Dai et al. [28] utilized a time-domain collocation technique in order to investigate the third-order superharmonic resonance in a Duffing oscillator. The adopted method could contribute to enhancing the non-physical solution dilemma, which appeared in high-dimension HB method. Huang et al. [29] applied a nonlinear isolator for achieving the vibration isolation based on Euler buckled beams to serve as negative stiffness corrector. They showed that the proposed isolator could behave like a softening, a softening–hardening, or a hardening system depending on the excitation force amplitude. Ozcelik and Attar [30] studied the influence of the damping and excitation frequency coefficients on the primary and superharmonic resonance responses in a cantilever beam with a flapping motion. The authors employed both Galerkin and perturbation techniques in order to extract the frequency-response relations of the superharmonic resonance case where a critical excitation amplitude could lead to bi-stable solutions. Sari [31] examined the superharmonic resonance of second and third orders in an Euler–Bernoulli beam where Eringen's nonlocal elasticity theory was utilized in the analysis. The author showed that the equilibrium amplitude could be affected by thermal loads, magnetic axial loads, and quadratic and cubic nonlinearities. Elliott et al. [32] used the methods of multiple time scales and direct normal-form for studying mechanical structures and showing their nonlinear dynamics. They assured that the approximate predictions obtained from the normal-form method were more accurate than that obtained from the multiple-scales method. Zhao et al. [33] discussed suspended cables with geometric nonlinearities inside thermal media where the secondary resonance with thermal effects were investigated. They studied four different cases of subharmonic and superharmonic resonances where a linear oscillatory behavior was present in some specific cooling/warming circumstances. Kandil [34] involved quintic nonlinearities in order to show the internal resonances amongst the discretized modes of a hinged-hinged Euler-Bernoulli beam. A Routh–Hurwitz criterion was fulfilled for showing the unstable solutions region of the first three modal deflections of the studied beam. Arena and Lacarbonara [35] investigated various resonance conditions with the multiple time-scales technique in thin elastic plates subjected to strain-induced excitation. Bifurcation diagrams were included to explain the resonance wide array caused by the harmonic excitation in nontrivial states of superharmonic resonance case. Kandil et al. [36] presented 2D and 3D plots of the frequency- and force-response curves of a controlled mass-damper-spring model for showing the influence of parameters variability on the system behavior. The whole controlled system dynamics were extracted thanks to Krylov–Bogoliubov averaging method, which helped to predict the very accurate behavior of the studied dynamical system. Su et al. [37] assembled a tuned mass damper with a cable in order to study the damper's participation in energy transfer from the cable to it and the nonlinear behavior of this transfer. With the aid of Galerkin technique and multiple-scales method, the authors proved analytically the important role that the tuned mass damper played in consuming and transferring the energy from the cable successfully. Long and Kang [38] investigated the nonlinear behavior of a carbon-fiber-reinforced polymer cable. They utilized the multiple-scales method in order to solve the governing differential equations that described the 1/3-order subharmonic resonance with 1:1 internal resonance of the studied cable. Kloda et al. [39] extracted a second-order approximate solution of a hinged-simply supported beam connected to axial spring with the aid of multiple-scales technique. They formulated different kinds of deformability and compared among them to make a conclusion about the exhibited strain energies. Kandil et al. [40] built an asymptotic analysis based on the Krylov–Bogoliubov averaging method in order to discuss the control performance of a mass-damper-spring model excited by a 1/3-order subharmonic resonance force. Guo and Rega [41] discussed the boundary-interior-coupled complex structures with an asymptotic analysis where the localized and global discretized modes of the studied structure were induced simultaneously once the modal frequencies were away from each other. Dalela et al. [42] fabricated a meta-structural isolation model connected to an equipment's isolation system where the excitation frequency was low. They adopted the HB method in order to plot the frequency-response relation and the steady-state motion transmissibility of the studied structure.

Based on the aforementioned papers, none of them discussed controlling the superharmonic resonance response via the cancelation of the cubic nonlinearity, which was the main motive to such a response. This control technique is proposed in the present work. This paper analyzes the secondary resonance of a nonlinear dynamical system in the form of a mass-damper-spring model under control. The adopted secondary resonance is the third-order superharmonic resonance where the excitation frequency is nearly one-third of the model's natural frequency. A cubic-position negative-velocity (CPNV) controller is applied for suppressing the unwanted oscillations of the studied model. Thanks to the harmonic balance technique, the whole-system dynamics is explained in both cases of deactivating or activating the controller. The solutions' stability can be checked with the aid of Floquet exponents.

2. Third-Order Superharmonic Resonance Analysis

Figure 1 represents a mass-damper-spring model, which is attached with a control unit in order to mitigate the unwanted oscillations $w(t)$ of the given car whose mass is M. Due to Newton's second law of motion, the horizontal displacement $w(t)$ is governed by the equation of motion:

$$M\ddot{w} + \mu\dot{w} + S_L w + S_{NL} w^3 = K\cos(\omega t) + F_c(t) \tag{1}$$

where μ is the damping factor of the given dashpot, S_L and S_{NL} are the linear and nonlinear stiffness of the given spring, K is the amplitude of the external excitation harmonic force, and $F_c(t)$ is the control force produced by the control unit.

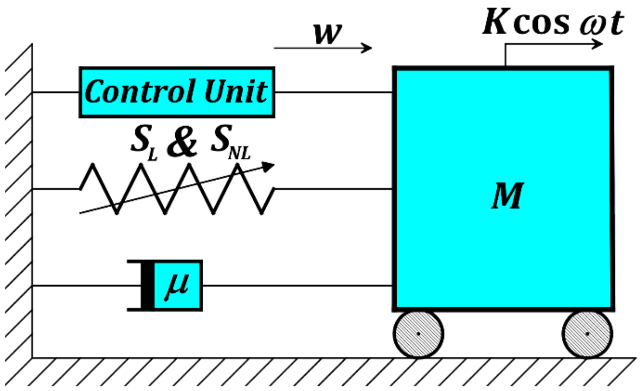

Figure 1. Mass-damper-spring model attached with a control unit.

As the car starts to oscillate under the influence of the external harmonic excitation $K\cos(\Omega t)$, these oscillatory displacements $w(t)$ are measured via the LVDT (linear variable differential transformer) shown in Figure 2a. The position of the LVDT's core determines the quantity of mutual inductance between the three coils depicted in the figure. Hence, the LVDT's output voltage V is produced proportional to the core's position. A signal conditioner role comes here in order to generate a suitable signal representing the original feedback signal $w(t)$. A CPNV (cubic-position negative-velocity) controller is adopted in this paper whose output control force is in the form $F_c(t) = K_p w^3 - K_v \dot{w}$. The CPNV controller is supplied with the w feedback signal that is cubed via a CUB (cuber) unit and then amplified by a K_p gain. The CUB block is shown in Figure 2b, where its function is built on the LOG and ANTILOG amplifiers. In addition, the w feedback signal is differentiated via a differentiator, then amplified by a K_v gain. Both of the gained signals are summed with the depicted signs in order to generate the control force F_c. After that, a power amplifier is utilized to equip the control signal F_c with the required power for driving the SCLA (servo-controlled linear actuator). This SCLA gives pull and push motions in order to do its job in the position control of the car.

Substituting $F_c(t) = K_p w^3 - K_v \dot{w}$ in Equation (1) and simplifying yield,

$$\ddot{w} + \zeta\dot{w} + \omega_n^2 w + \beta w^3 = k\cos(\omega t) + k_p w^3 - k_v \dot{w} \tag{2}$$

where $\zeta = \mu M^{-1}$, $\omega_n^2 = S_L M^{-1}$, $\beta = S_{NL} M^{-1}$, $k = K M^{-1}$, $k_p = K_p M^{-1}$, and $k_v = K_v M^{-1}$. The exact solution of Equation (2) cannot be extracted with the well-known calculus theories, so we should resort to obtaining the approximate solution via one of the approximation theories known as the harmonic balance (HB) method [43]. We have worked in previously published papers with different analytical perturbation techniques, such as multiple-scales method and Krylov–Bogoliubov averaging method, for extracting the first-order approximate solution. In this work, we adopted the HB analysis for diversity, as it can give us the same first-order approximation gained by the aforementioned methods. We seek a superharmonic resonance solution where ω is away from ω_n (especially where $\omega_n \cong 3\omega$), which occurs due to a hard excitation force. Hence, an approximate equilibrium solution of Equation (2) can be assumed in the form

$$\begin{aligned} w_0 &= 2\Lambda\cos(\omega t) + \sum_{j=1}^{\infty}\left[P_j\cos(j\omega_n t) + Q_j\sin(j\omega_n t)\right] \\ &\cong 2\Lambda\cos(\omega t) + P_1\cos(3\omega t) + Q_1\sin(3\omega t) \end{aligned} \tag{3}$$

where the first term is the particular integral solution to the linear hard-forced un-damped problem $\ddot{w} + \omega_n^2 w = k\cos(\omega t)$ and $2\Lambda = k\left(\omega_n^2 - \omega^2\right)^{-1}$, while the summation refers to the harmonic series of ω_n as a solution to the linear free un-damped problem $\ddot{w} + \omega_n^2 w = 0$. For simplicity, an approximation was performed in Equation (3) by taking only the fundamental terms of the series (at $j = 1$), then replacing $\omega_n \cong 3\omega$ because we only care about the third-order superharmonic analysis in this study. We therefore substitute Equation (3) into Equation (2) to obtain

$$\begin{aligned} &\left[\left(\beta - k_p\right)\left(3\Lambda^2 P_1 + 6\Lambda^3 + 3\Lambda\left(P_1^2 + Q_1^2\right)\right) + 2\Lambda\left(\omega_n^2 - \omega^2\right) - k\right]\cos(\omega t) \\ &\quad + \left[3\Lambda^2 Q_1\left(\beta - k_p\right) - 2\omega\Lambda(\zeta + k_v)\right]\sin(\omega t) \\ &\quad + \left[\left(\omega_n^2 - 9\omega^2\right)P_1 + \left(\beta - k_p\right)\left(\tfrac{3}{4}\left(P_1^3 + P_1 Q_1^2\right) + 6\Lambda^2 P_1 + 2\Lambda^3\right)\right. \\ &\quad \left. + 3\omega Q_1(\zeta + k_v)\right]\cos(3\omega t) \\ &\quad + \left[\left(\omega_n^2 - 9\omega^2\right)Q_1 + \left(\beta - k_p\right)\left(\tfrac{3}{4}\left(Q_1^3 + P_1^2 Q_1\right) + 6\Lambda^2 Q_1\right)\right. \\ &\quad \left. - 3\omega P_1(\zeta + k_v)\right]\sin(3\omega t) + HOH = 0 \end{aligned} \tag{4}$$

where the HOH refers to undesired harmonics of high orders. Let us represent P_1 and Q_1 in polar form as

$$P_1 + iQ_1 = ae^{i\gamma} = a(\cos\gamma + i\sin\gamma) \tag{5}$$

where a and γ are the amplitude and phase of the car's motion, respectively. Inserting Equation (5) into Equation (4) with selecting only the coefficients of $\cos(3\omega t)$ and $\sin(3\omega t)$ on both sides of Equation (4), as we care about the third-order superharmonic resonance case:

$$\begin{aligned} &\left(\omega_n^2 - 9\omega^2\right)a\cos\gamma + \left(\beta - k_p\right)\left(\tfrac{3}{4}a^3\cos\gamma + 6\Lambda^2 a\cos\gamma + 2\Lambda^3\right) + 3\omega a(\zeta + k_v)\sin\gamma \\ &\quad = 0 \end{aligned} \tag{6a}$$

$$\left(\omega_n^2 - 9\omega^2\right)a\sin\gamma + \left(\beta - k_p\right)\left(\frac{3}{4}a^3\sin\gamma + 6\Lambda^2 a\sin\gamma\right) - 3\omega a(\zeta + k_v)\cos\gamma = 0 \tag{6b}$$

Next, we multiply Equation (6a) by $\sin\gamma$ and Equation (6b) by $-\cos\gamma$ and then add the new equations yield Equation (7a). Similarly, we multiply Equation (6a) by $\cos\gamma$ and Equation (6b) by $\sin\gamma$ and then add the new equations yield Equation (7b). The manipulated Equations (6a) and (6b) can have the new form in Equations (7a) and (7b) as follows:

$$3\omega a(\zeta + k_v) + 2\Lambda^3\sin\gamma\left(\beta - k_p\right) = 0 \tag{7a}$$

$$\left(\omega_n^2 - 9\omega^2\right)a + \left(\beta - k_p\right)\left(\frac{3}{4}a^3 + 6\Lambda^2 a + 2\Lambda^3\cos\gamma\right) = 0 \tag{7b}$$

Next, extract $\sin\gamma$ from Equation (7a) and $\cos\gamma$ from Equation (7b), then square, and add the new equations, which leads us to eliminate γ from Equation (7) as follows

$$9(\zeta + k_v)^2\omega^2 a^2 + \left[\omega_n^2 - 9\omega^2 + \left(\beta - k_p\right)\left(6\Lambda^2 + \tfrac{3}{4}a^2\right)\right]^2 a^2 = 4\Lambda^6\left(\beta - k_p\right)^2 \ c \tag{8}$$

The equation above represents the relationship between the amplitude a and different system parameters with the absence of the phase γ. Rearranging Equation (8) yields the following sextic equation in terms of a:

$$\frac{9\left(\beta-k_p\right)^2}{16}a^6+\frac{3\left(\beta-k_p\right)}{2}\left(\omega_n^2-9\omega^2+6\Lambda^2\left(\beta-k_p\right)\right)a^4$$
$$+\left[9\left(\zeta+k_v\right)^2\omega^2+\left(\omega_n^2-9\omega^2+6\Lambda^2\left(\beta-k_p\right)\right)^2\right]a^2-4\Lambda^6\left(\beta-k_p\right)^2=0 \tag{9}$$

(**a**)

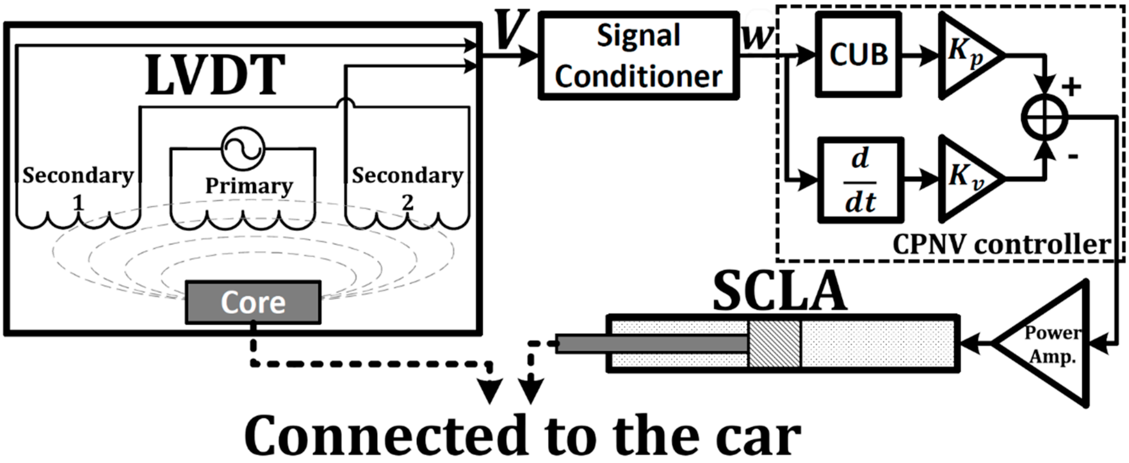

(**b**)

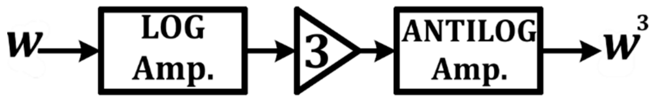

Figure 2. Block diagrams of: (**a**) the control unit and (**b**) the cuber (CUB) unit.

The equilibrium amplitude a computed from the equation above should be tested for local stability. Hence, the assumed steady-state solution w_0 can be superposed by a small change w_1 on it such that the general solution is $w=w_0+w_1$. This assumption is substituted into Equation (2), knowing that w_0 has previously satisfied Equation (2), then keeping the linear terms only in w_1 to have

$$\ddot{w}_1+(\zeta+k_v)\dot{w}_1+\omega_n^2w_1+3\left(\beta-k_p\right)w_0^2w_1=0 \tag{10}$$

Due to the term w_0^2, the above equation has a variable coefficient where its local stability resembles the local stability of the equilibrium solution $w_0=a\cos(3\omega t-\gamma)+2\Lambda\cos(\omega t)$. According to Floquet theory, the solution to Equation (10) may be expressed as

$$w_1=e^{\alpha\tau}z \tag{11}$$

where α refers to the Floquet exponent, while z is a periodic function of period $2\pi/3\omega$. Substituting Equation (11) into Equation (10) leads to

$$\ddot{z}+(2\alpha+\zeta+k_v)\dot{z}+\left(\alpha^2+(\zeta+k_v)\alpha+\omega_n^2+3\left(\beta-k_p\right)w_0^2\right)z=0 \tag{12}$$

The free oscillatory solution z to Equation (12) can be assumed in the form

$$z=A_1\cos(3\omega t)+B_1\sin(3\omega t) \tag{13}$$

where A_1 and B_1 have been supposed differently of P_1 and Q_1 in Equation (3). Inserting Equation (13) into Equation (12) with selecting only the coefficients of $\cos(3\omega t)$ and $\sin(3\omega t)$ can lead us to

$$\begin{bmatrix}\delta_{11} & \delta_{12}\\ \delta_{21} & \delta_{22}\end{bmatrix}\begin{bmatrix}A_1\\ B_1\end{bmatrix}=\begin{bmatrix}0\\ 0\end{bmatrix} \tag{14}$$

where

$$\delta_{11} = \alpha^2 + \omega_n^2 - 9\omega^2 + (\zeta + k_v)\alpha + 6(\beta - k_p)\Lambda^2 + \frac{3(\beta - k_p)}{4}a^2[\cos(2\gamma) + 2]$$
$$\delta_{12} = 6\alpha\omega + 3\omega(\zeta + k_v) + \frac{3(\beta - k_p)}{4}a^2\sin(2\gamma)$$
$$\delta_{21} = -\delta_{12} + \frac{3(\beta - k_p)}{2}a^2\sin(2\gamma)$$
$$\delta_{22} = \delta_{11} - \frac{3(\beta - k_p)}{2}a^2\cos(2\gamma)$$

Setting the determinant of Equation (14)'s coefficient matrix equal to zero will give us a characteristic equation in terms of α. The small change w_1 and thus the steady-state solution w_0 will be asymptotically stable if and only if all of the real parts of α are negative, and the solution will be unstable otherwise.

3. Superharmonic Resonance Curves and Discussion

Before plotting the curves, the adopted values of the physical system parameters during operation are presented as follows: the damping coefficient as $\zeta = 0.02\ \mathrm{s}^{-1}$, the system's natural angular frequency as $\omega_n = 3.1623$ rad/s, the cubic-nonlinearity coefficient as $\beta = 0.8\ \mathrm{m}^{-2}\mathrm{s}^{-2}$, the exciting force amplitude as $k = 7$ N/kg, the exciting force angular frequency as $\omega \cong \omega_n/3$ rad/s, the cubic-position (CP) control gain as $k_p = 0.8\ \mathrm{m}^{-2}\mathrm{s}^{-2}$, and the negative-velocity (NV) control gain as $k_v = 0.02\ \mathrm{s}^{-1}$. Due to the upcoming analysis, some of the stated constants may be changed for necessity. The relation of the car's oscillation amplitude a (measured in meters) vs. both the excitation frequency ω and its amplitude k pre-control ($k_p = k_v = 0$) is plotted in Figure 3. Figure 3a depicts the 2D curves of a vs. ω at different values of k ={4, 5, 6, 7}. It is shown that the greater k is, the more the curves rise and bend to the right with a small right shift of the whole curve due to the domination of the cubic nonlinearity. For clarity, the solid paths refer to the stable solutions paths, while the light-color paths refer to the unstable solutions branches. The light-color paths extend proportionally, with the parameter k leading to a more severe jump from the curve's peak to the lower values on the same curve. These jumps happen at the vertical tangency points (Saddle–Node bifurcation points) where the stable and unstable paths collide. Moreover, the process is clear on the 3D surface in Figure 3b in which the relation of a is plotted instantly against ω and k as an analogy to the curves plotted in Figure 3a. The reader should be aware that the surface's red color refers to maximum function values, while the blue color refers to minimum functions values in Figure 3b. Figure 4 shows the relation of the car's oscillation amplitude a vs. both the excitation frequency ω and the damping coefficient ζ pre-control ($k_p = k_v = 0$). It can be seen that the damping ζ can help in suppressing the curve's peak that leads to a shorter unstable path and a lower possibility of encountering jumps along the curve. This can be clearly seen on the green curve ($\zeta = 0.05$) where the curve's entire path is stable without any jumps or unstable paths. In Figure 5, the relation of the car's oscillation amplitude a vs. both the excitation frequency ω and the cubic-nonlinearity factor β pre-control ($k_p = k_v = 0$) is plotted. Anyone can see that raising value of β positively (or negatively) forces the curve to bend more to the right (or to the left) due to the hardening-type (or the softening-type) spring. Furthermore, the lower the value of β is, the lower the curve's peak becomes. This can guide us to the idea of the controller used in this work that depends on cancelling the nonlinearity effect in order to suppress the car's oscillation peaks.

The relationship of the car's oscillation amplitude a vs. both the excitation amplitude k and its frequency ω is pictured in Figure 6 pre-control ($k_p = k_v = 0$). When $\omega = \omega_n/3 = 1.0541$ rad/s, the black curve shows that car's oscillatory amplitude a responds linearly with small values to the excitation amplitude k. There are no unstable paths on the curve. When ω increases to $\omega = 1.06$ rad/s, the red curve exhibits a peak at $k \cong 3\frac{\mathrm{N}}{\mathrm{kg}}$, but the behavior is still linear with a quite small slope and no unstable paths. As ω increases on the blue, green, and cyan curves, the nonlinear behavior starts to appear with unstable paths that increase gradually from one curve to another one. The possibility of jumping increases with ω until it becomes severe, as shown on the cyan curve. Figure 7 declares the relationship of the car's oscillation amplitude a vs. both the excitation amplitude k and the damping factor ζ pre-control ($k_p = k_v = 0$). The damping effect is present by increasing ζ where the curve's peak is reduced. This can give us a key to damp the behavior of the car's oscillations by adopting a controller that enhances the damping effect. Furthermore, the relation of the car's oscillation amplitude a vs. the excitation amplitude k and the cubic-nonlinearity parameter β is depicted in Figure 8 pre-control ($k_p = k_v = 0$). This is also a way to another control key of adjusting the value of β where decreasing it can extend the k-range of minimum car's amplitudes as shown in the figure.

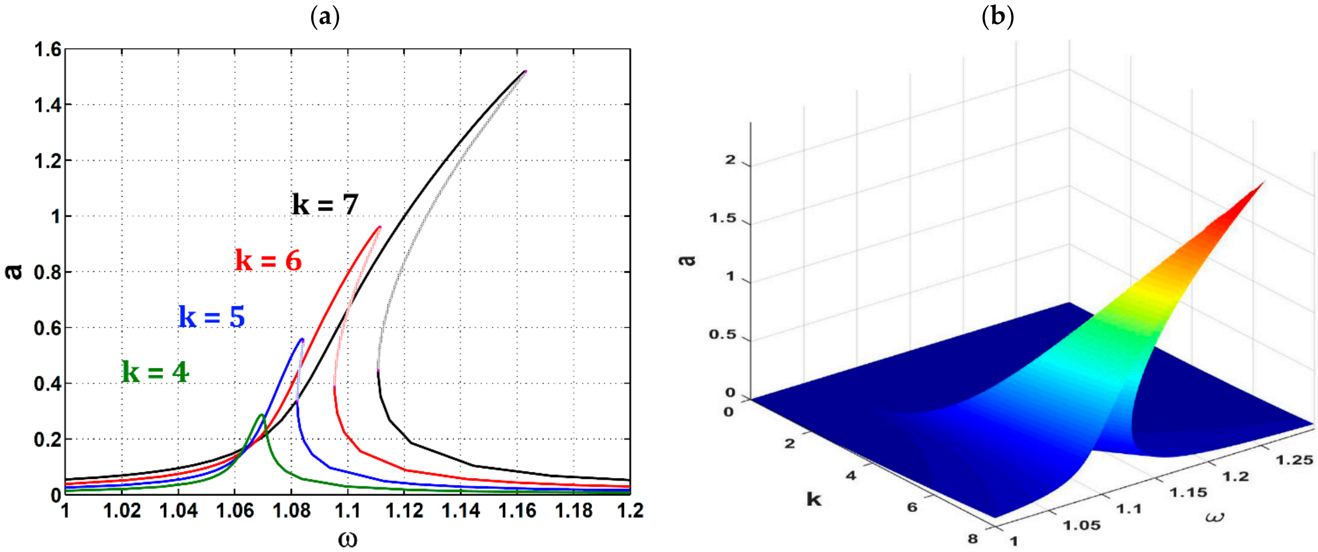

Figure 3. Relationship between the car's oscillation amplitude a and (**a**) the excitation frequency ω at different values of excitation amplitude k, (**b**) both the excitation frequency ω and its amplitude k, at $\zeta = 0.02$ and $\beta = 0.8$ pre-control ($k_p = k_v = 0$).

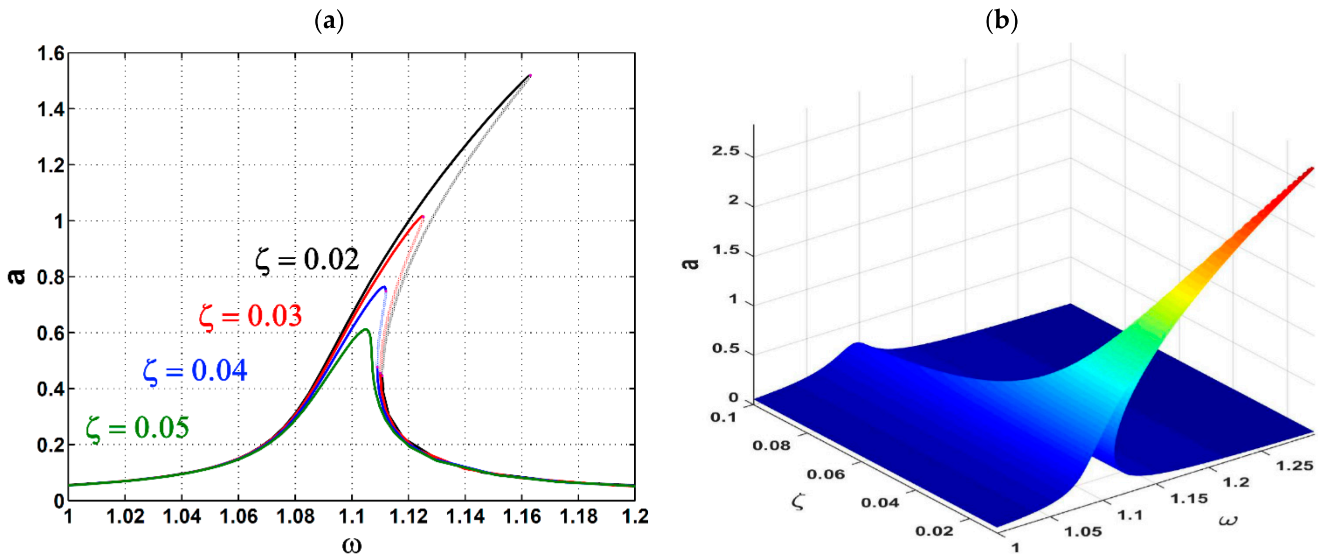

Figure 4. Relationship between the car's oscillation amplitude a and (**a**) the excitation frequency ω at different values of damping factor ζ, (**b**) both the excitation frequency ω and damping factor ζ, at $k = 7$ and $\beta = 0.8$ pre-control ($k_p = k_v = 0$).

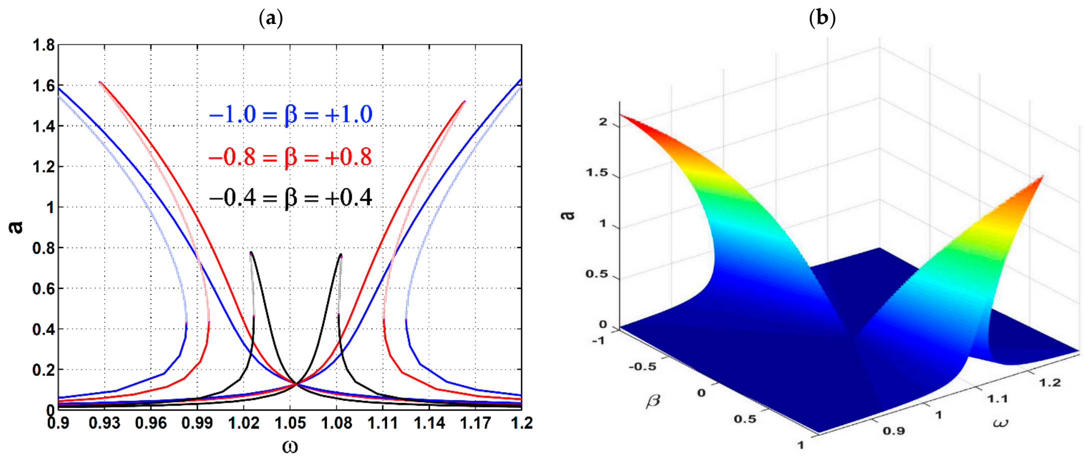

Figure 5. Relationship between the car's oscillation amplitude a and (**a**) the excitation frequency ω at different values of cubic-nonlinearity factor β, (**b**) both the excitation frequency ω and cubic-nonlinearity factor β, at $\zeta = 0.02$ and $k = 7$ pre-control ($k_p = k_v = 0$).

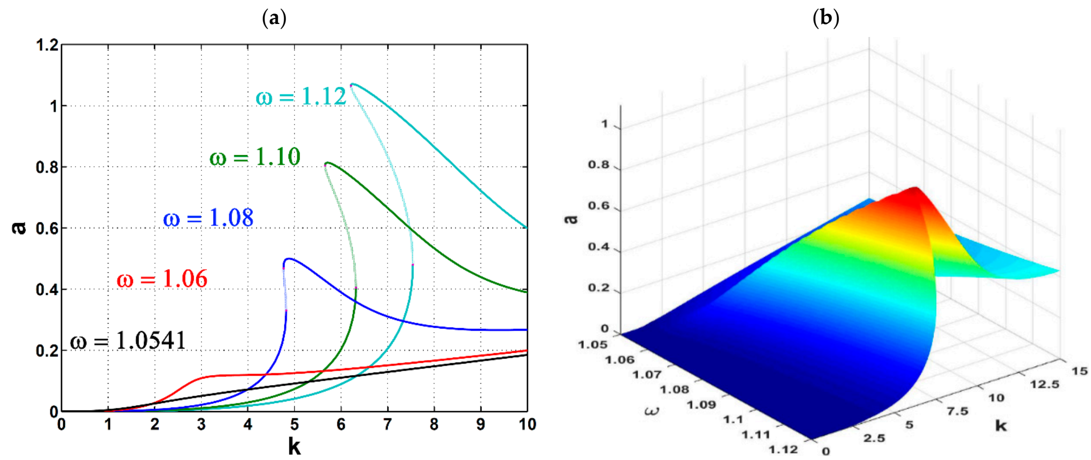

Figure 6. Relationship between the car's oscillation amplitude a and (**a**) the excitation amplitude k at different values of excitation frequency ω, (**b**) both the excitation amplitude k and its frequency ω, at $\zeta = 0.02$ and $\beta = 0.8$ pre-control ($k_p = k_v = 0$).

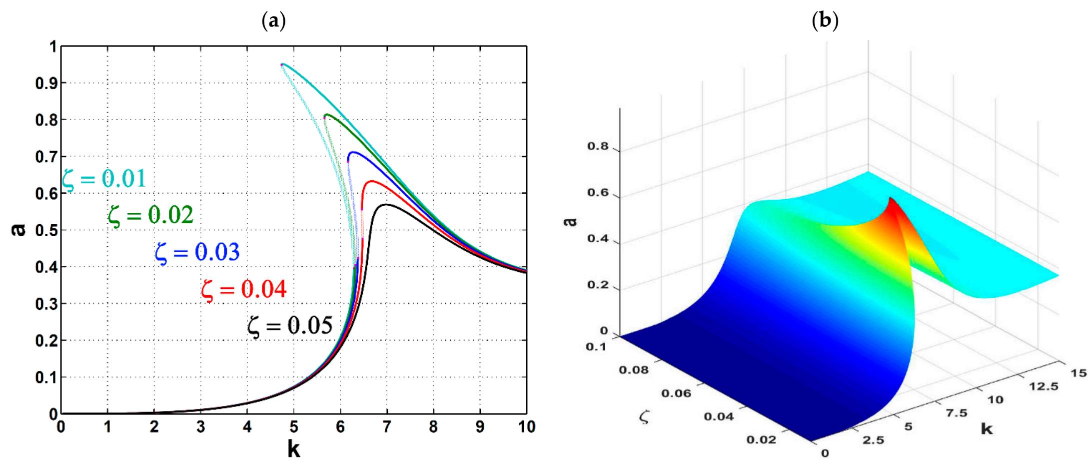

Figure 7. Relationship between the car's oscillation amplitude a and (**a**) the excitation amplitude k at different values of damping factor ζ, (**b**) both the excitation amplitude k and damping factor ζ, at $\omega = 1.1$ and $\beta = 0.8$ pre-control ($k_p = k_v = 0$).

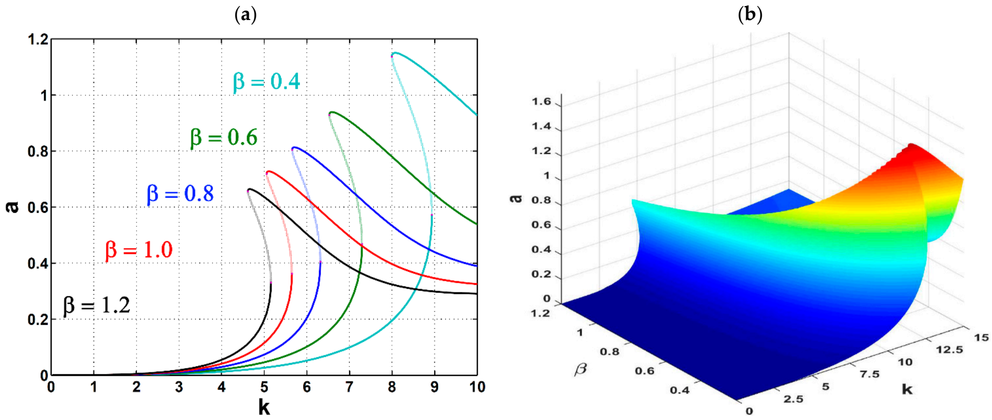

Figure 8. Relationship between the car's oscillation amplitude a and (**a**) the excitation amplitude k at different values of cubic-nonlinearity parameter β, (**b**) both the excitation amplitude k and cubic-nonlinearity parameter β, at $\zeta = 0.02$ and $\omega = 1.1$ pre-control ($k_p = k_v = 0$).

Activation of the control unit is discussed and plotted in Figures 9–12 with different adopted values of both the CP control gain k_p and the NV control gain k_v. The relationship of the car's oscillation amplitude a vs. the excitation frequency ω and the CP control gain k_p is portrayed in Figure 9 post-control but at $k_v = 0$. As shown above in Figure 5, the reduction of β could suppress the curve's peak and force it to turn linear without any unstable paths. Based on Equation (9), raising the parameter k_p in the bracket $(\beta - k_p)$ can cause the reduction in the whole cubic-nonlinearity term as shown in Figure 9. Reaching the value $k_p = \beta = 0.8$ can modify Equation (9) as follows:

$$\left[9(\zeta + k_v)^2\omega^2 + \left(\omega_n^2 - 9\omega^2\right)^2\right]a^2 = 0 \tag{15}$$

which yields the zero-amplitude solution (trivial solution), i.e., $a = 0$. This is obvious in the figure where the cyan curve represents the trivial amplitude in the case that $k_p = 0.8 = \beta$. Moreover, Figure 10 shows the relationship of the car's oscillation amplitude a vs. the excitation frequency ω and the NV control gain k_v post-control but at $k_p = 0.6$. The parameter k_v is very helpful in improving the damping behavior as discussed above in Figure 4. In addition, Figures 11 and 12 demonstrate the effect of k_p and k_v on the relationship between the car's amplitude a and the force amplitude k, similar to the way they were shown above in Figures 7 and 8. The reader can notice that also $k_p = 0.8 = \beta$ can make the car follow the trivial amplitude path ($a = 0$) regardless the value of k. The parameter k_v helps in enhancing the overall damping behavior of the car's oscillations as well.

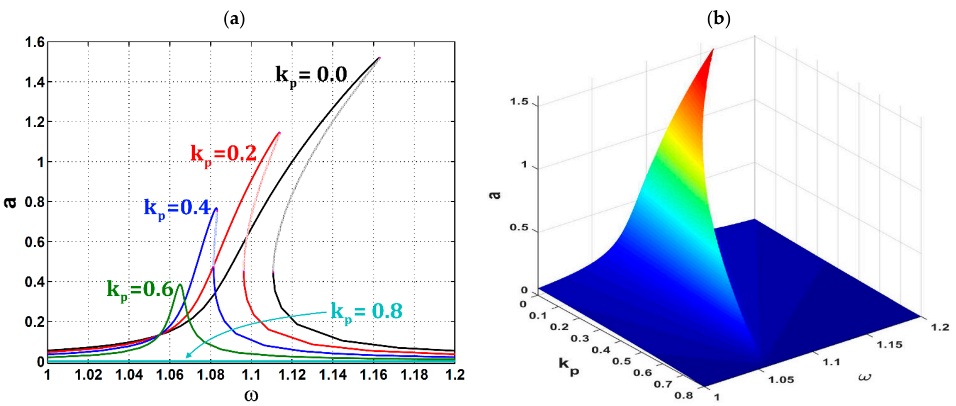

Figure 9. Relationship between the car's oscillation amplitude a and (**a**) the excitation frequency ω at different values of CP control gain k_p, (**b**) both the excitation frequency ω and CP control gain k_p post-control ($k_v = 0$).

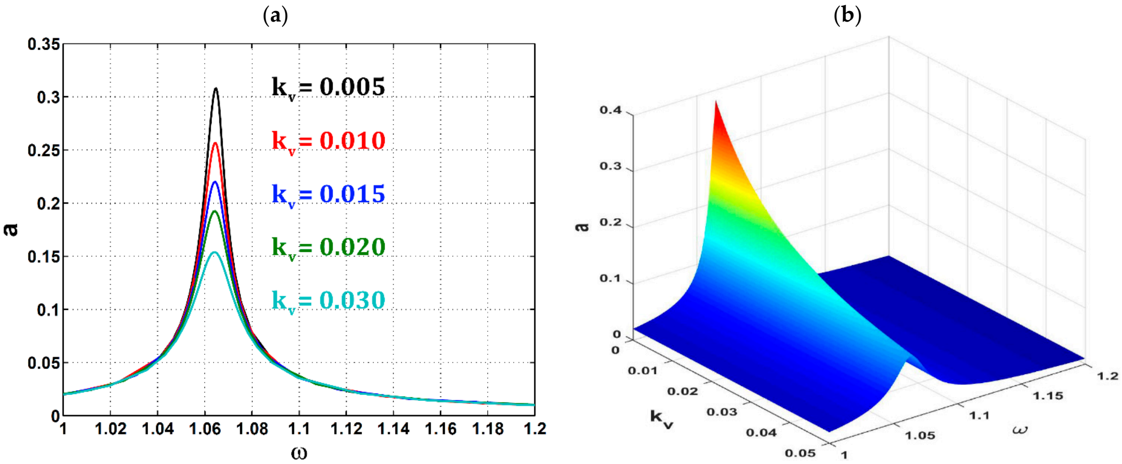

Figure 10. Relationship between the car's oscillation amplitude a and (**a**) the excitation frequency ω at different values of NV control gain k_v, (**b**) both the excitation frequency ω and NV control gain k_v post-control ($k_p = 0.6$).

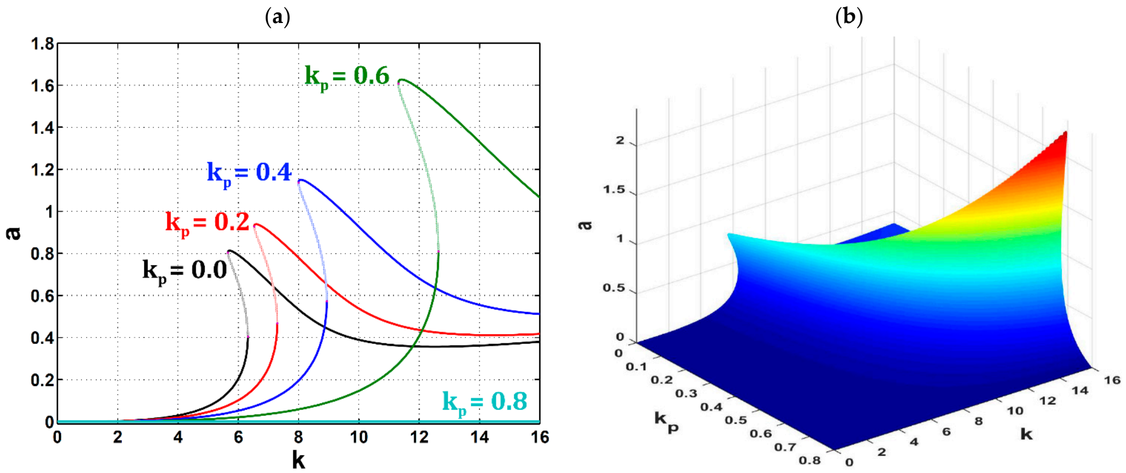

Figure 11. Relationship between the car's oscillation amplitude a and (**a**) the excitation amplitude k at different values of CP control gain k_p, (**b**) both the excitation amplitude k and CP control gain k_p post-control ($k_v = 0$).

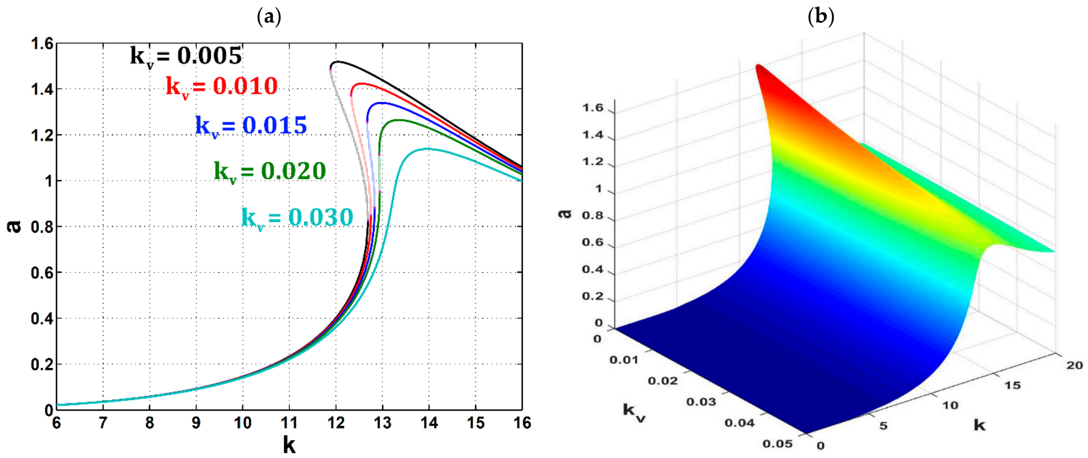

Figure 12. Relationship between the car's oscillation amplitude a and (**a**) the excitation amplitude k at different values of NV control gain k_v, (**b**) both the excitation amplitude k and NV control gain k_v post-control ($k_p = 0.6$).

Figures 13–15 present the time history of the car pre-control (Figure 13) and post-control (Figures 14 and 15). These figures have been plotted adopting the well-known fourth-order Runge–Kutta numerical algorithm. Figure 13 shows the behavior before control at $\omega = 1.12$, $k = 7$, $\beta = 0.8$, $\zeta = 0.02$, and $k_p = k_v = 0$ for a total operation time of 600 s as in Figure 13a and for the last 50 s of the total operation time as in Figure 13b. It is clear that the oscillations become steady after about 400 s, and that will be treated later. Figure 14 is showing the behavior after control at $\omega = 1.12$, $k = 7$, $\beta = 0.8$, $\zeta = 0.02$, $k_p = 0.8$, and $k_v = 0$ for a total operation time of 600 s as in Figure 14a and for the last 50 s of the total operation time as in Figure 14b. It can be seen that the oscillations have been mitigated by about 90% from its former state thanks to the applied controller. In addition, the transient oscillations end after about 250 s, which is an advantage. Figure 15 shows the behavior after control similarly as in Figure 14 except for $k_v = 0.02$. The reader can notice that the transient oscillations end after about 150 s, which is an improvement over the case where $k_v = 0$ in Figure 14. The steady oscillations are not affected by adjusting k_v as this parameter enhances the transient state in case the parameter k_p is kept at 0.8. Finally, Figure 16 clarifies the comparison between the analytical solution approached by the harmonic balance (HB) method and the numerical solution approached by the fourth-order Runge–Kutta (RK4) method. The HB solution is represented by solid curves, while the RK4 solution is represented by circles (for sweeping the parameter up) and dots (for sweeping the parameter down). Figure 16a shows a comparison for a frequency-response curve (a vs. ω) in case of $k = 7$ before and after control. We can see that there is a good agreement between the two methods before control. After control, the trivial HB solution (acts as the theoretical solution) deviates a little bit from the trivial RK4 solution (acts as practical solution), but it maintains its trend the same way as the trivial HB solution during varying ω. Figure 16b shows a comparison for a force-response curve (a vs. k) in case of $\omega = 1.1$ before and after control. There is still a good agreement between the two approaches before and after control in case of low values of the force k, while they deviate from each other a little bit as the force k increases as shown due to the excessive force that energizes the car's motion.

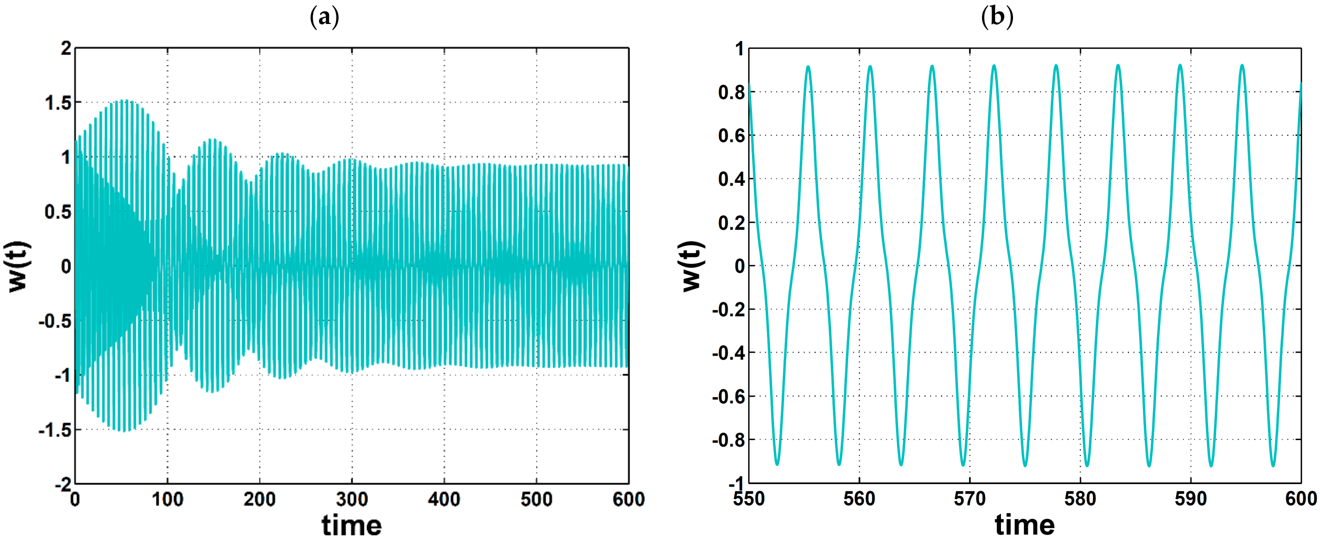

Figure 13. The time history of the car pre-control ($k_p = k_v = 0$) at $\omega = 1.12$, $k = 7$, $\beta = 0.8$, and $\zeta = 0.02$: (**a**) total trace for 600 s and (**b**) last 50 s of the total trace.

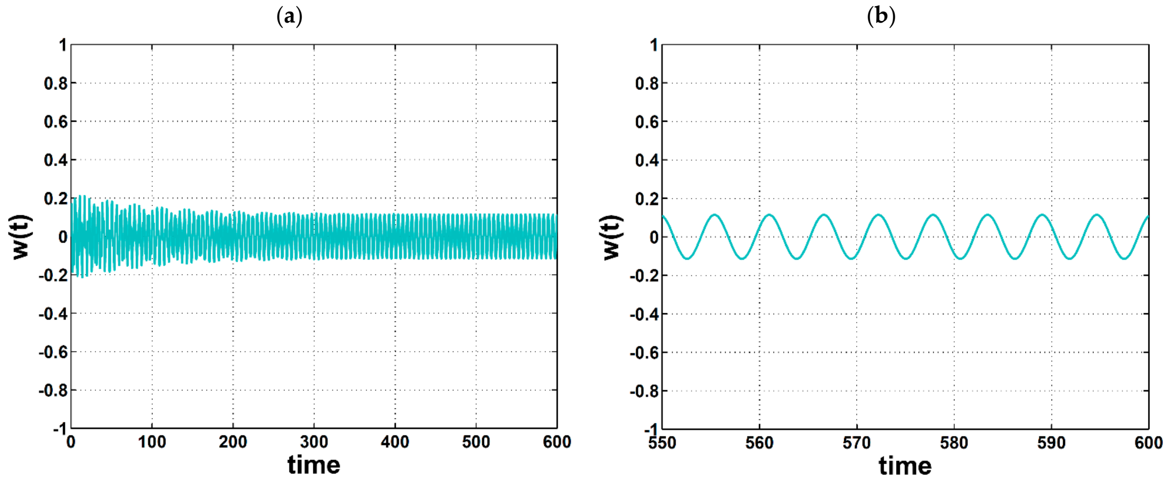

Figure 14. The time history of the car post-control ($k_p = 0.8$ and $k_v = 0$) at $\omega = 1.12$, $k = 7$, $\beta = 0.8$, and $\zeta = 0.02$: (**a**) total trace for 600 s and (**b**) last 50 s of the total trace.

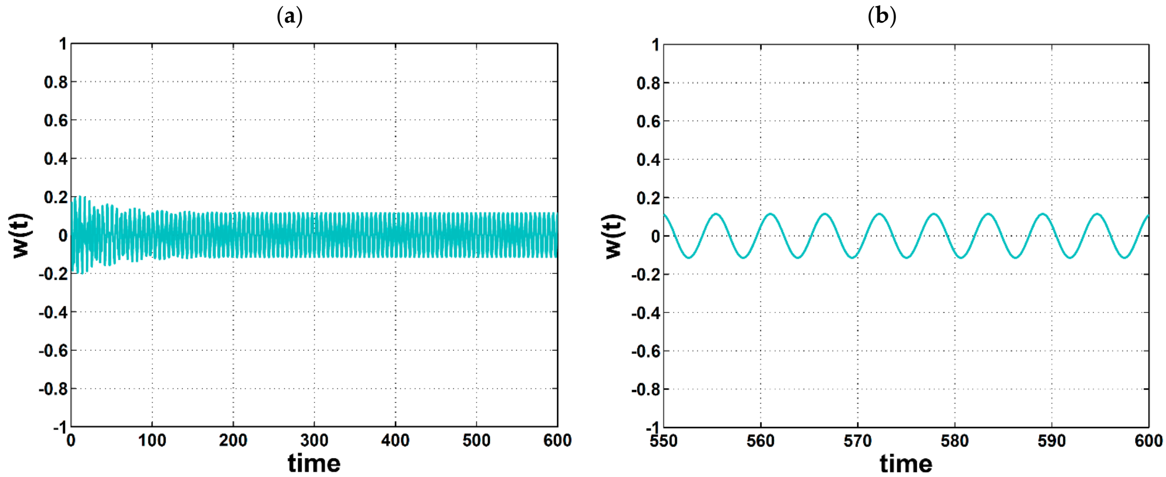

Figure 15. The time history of the car post-control ($k_p = 0.8$ and $k_v = 0.02$) at $\omega = 1.12$, $k = 7$, $\beta = 0.8$, and $\zeta = 0.02$: (**a**) total trace for 600 s and (**b**) last 50 s of the total trace.

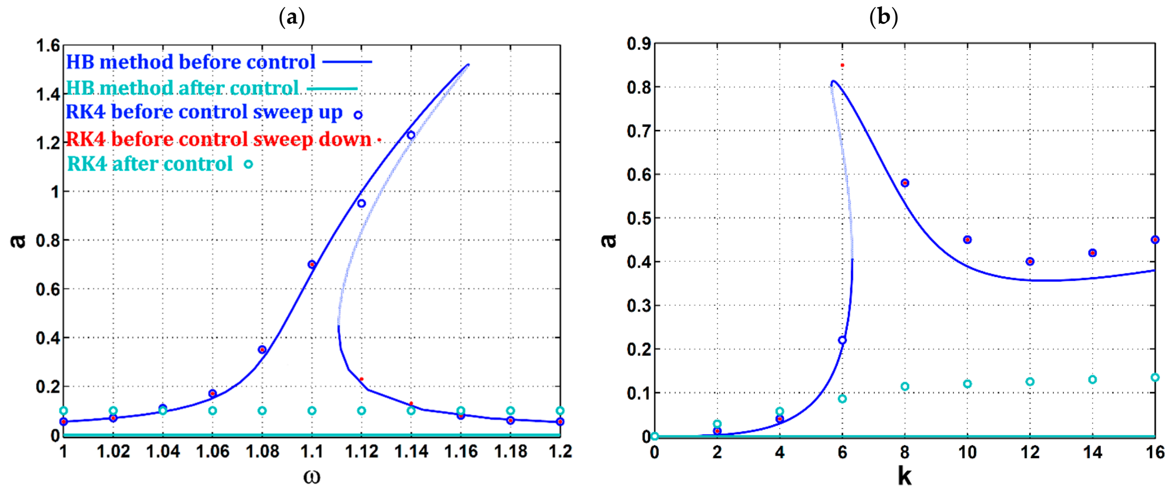

Figure 16. A comparison between the HB analytical solution (solid curves) and the RK4 numerical solution (circles and dots): (**a**) frequency-response curve a vs. ω at $k = 7$ and (**b**) force-response curve a vs. k at $\omega = 1.1$.

4. Concluding Remarks

The present work analyzed the secondary resonance analysis of a nonlinear dynamical system in the form of a controlled mass-damper-spring model. The secondary resonance in this work was a third-order superharmonic resonance where the excitation frequency ω is in the vicinity of one-third of the model's natural frequency ω_n. A CPNV controller was applied in order to suppress the car's unwanted oscillations. The whole system dynamics was explained pre- and post-control thanks to the harmonic balance method. Floquet exponents were utilized so we could check the solutions' stability. The following remarks are given as a concluding summary of this research:

- The greater the excitation amplitude k was, the more the frequency response curves rose and bent to the right with a slight right shift of the whole curve due to the domination of the cubic nonlinearity.
- The unstable solutions paths extended proportionally, with k leading to a more severe jump from the curve's peak to the lower values on the same curve.
- The damping coefficient ζ could help in suppressing the curve's peak that led to a shorter unstable path and a lower possibility of encountering jumps along the curve.
- Raising the value of the cubic-nonlinearity coefficient β positively (or negatively) forced the curve to bend more to the right (or to the left) due to the hardening-type (or the softening-type) spring.
- The lower the value of β, the lower the curve's peak became.
- As the excitation frequency ω increased, the nonlinear behavior of the force-response curves started to appear with unstable paths that increased gradually from one curve to another one.
- Raising the CP control gain k_p could cause a reduction in the whole cubic-nonlinearity term leading to suppressing the curve's peak.
- The trivial car's amplitude $a = 0$ could be reached theoretically in the case that $k_p = \beta$ regardless the value of k.
- The NV control gain k_v helped in enhancing the overall damping behavior of the car's oscillations.
- The car's steady oscillations were mitigated by about 90% from its former state thanks to the applied controller.
- The car's transient oscillations ended faster than its former state thanks to the applied controller.

Author Contributions: Conceptualization, A.K., Y.S.H., M.S.M., J.A. and M.B.; methodology, A.K., Y.S.H., M.S.M., J.A. and M.B.; software, A.K.; validation, A.K., Y.S.H., M.S.M., J.A. and M.B.; formal analysis, A.K.; investigation, A.K.; resources, A.K.; data curation, A.K.; writing—original draft preparation, A.K.; writing—review and editing, A.K.; visualization, A.K. All authors have read and agreed to the published version of the manuscript.

Funding: This research received no external funding.

Institutional Review Board Statement: Not applicable.

Informed Consent Statement: Not applicable.

Data Availability Statement: Not applicable.

Acknowledgments: This research was supported by Taif University Researchers Supporting Project Number (TURSP-2020/160), Taif University, Taif, Saudi Arabia. This research was also supported by the National Science Centre, Poland, under the grant OPUS 14 No. 2017/27/B/ST8/01330.

Conflicts of Interest: The authors declare no conflict of interest.

References

1. Rahman, Z.; Burton, T.D. Large amplitude primary and superharmonic resonances in the Duffing oscillator. *J. Sound Vib.* **1986**, *110*, 363–380. [CrossRef]
2. Nayfeh, A.H.; Sanchez, N.E. Bifurcations in a forced softening duffing oscillator. *Int. J. Non-Linear Mech.* **1989**, *24*, 483–497. [CrossRef]

3. Benedettini, F.; Rega, G. Planar non-linear oscillations of elastic cables under superharmonic resonance conditions. *J. Sound Vib.* **1989**, *132*, 353–366. [CrossRef]
4. Burton, T.D.; Anderson, M. On asymptotic behavior in cascades chaotically excited non-linear oscillators. *J. Sound Vib.* **1989**, *133*, 353–358. [CrossRef]
5. Rahman, Z.; Burton, T.D. On higher order methods of multiple scales in non-linear oscillations-periodic steady state response. *J. Sound Vib.* **1989**, *133*, 369–379. [CrossRef]
6. Sanchez, N.E.; Nayfeh, A.H. Prediction of bifurcations in a parametrically excited duffing oscillator. *Int. J. Non-Linear Mech.* **1990**, *25*, 163–176. [CrossRef]
7. Rega, G.; Benedettini, F.; Salvatori, A. Periodic and chaotic motions of an unsymmetrical oscillator in nonlinear structural dynamics. *Chaos Solitons Fractals* **1991**, *1*, 39–54. [CrossRef]
8. Gottlieb, O.; Yim, S.C.S. Nonlinear oscillations, bifurcations and chaos in a multi-point mooring system with a geometric nonlinearity. *Appl. Ocean Res.* **1992**, *14*, 241–257. [CrossRef]
9. Hamdan, M.N.; Burton, T.D. On the Steady State Response and Stability of Non-Linear Oscillators Using Harmonic Balance. *J. Sound Vib.* **1993**, *166*, 255–266. [CrossRef]
10. Hassan, A. On the Third Superharmonic Resonance in the Duffing Oscillator. *J. Sound Vib.* **1994**, *172*, 513–526. [CrossRef]
11. Addison, P.S. On the characterization of non-linear oscillator systems in chaotic mode. *J. Sound Vib.* **1995**, *179*, 385–398. [CrossRef]
12. Adrezin, R.; Bar-Avi, P.; Benaroya, H. Dynamic Response of Compliant Offshore Structures—Review. *J. Aerosp. Eng.* **1996**, *9*, 114–131. [CrossRef]
13. Lukomsky, V.P.; Bobkov, V.B. Asymptotic Expansions of the Periodic Solutions of Nonlinear Evolution Equations. *Nonlinear Dyn.* **1998**, *16*, 1–21. [CrossRef]
14. Vaidya, P.G.; He, R. An analysis of the trans-spectral-coherence for duffing oscillators undergoing chaos. *J. Sound Vib.* **1998**, *212*, 435–454. [CrossRef]
15. Luongo, A.; Paolone, A. On the Reconstitution Problem in the Multiple Time-Scale Method. *Nonlinear Dyn.* **1999**, *19*, 135–158. [CrossRef]
16. Al-Qaisia, A.A.; Hamdan, M.N. On the steady state response of oscillators with static and inertia non-linearities. *J. Sound Vib.* **1999**, *223*, 49–71. [CrossRef]
17. Khanin, R.; Cartmell, M.; Gilbert, A. A computerised implementation of the multiple scales perturbation method using Mathematica. *Comput. Struct.* **2000**, *76*, 565–575. [CrossRef]
18. Hamdan, M.N.; Al-Qaisia, A.A.; Al-Bedoor, B.O. Comparison of analytical techniques for nonlinear vibrations of a parametrically excited cantilever. *Int. J. Mech. Sci.* **2001**, *43*, 1521–1542. [CrossRef]
19. Nielsen, S.R.K.; Kirkegaard, P.H. Super and combinatorial harmonic response of flexible elastic cables with small sag. *J. Sound Vib.* **2002**, *251*, 79–102. [CrossRef]
20. Cartmell, M.P.; Ziegler, S.W.; Khanin, R.; Forehand, D.I.M. Multiple scales analyses of the dynamics of weakly nonlinear mechanical systems. *Appl. Mech. Rev.* **2003**, *56*, 455–492. [CrossRef]
21. Rega, G. Nonlinear vibrations of suspended cables—Part I: Modeling and analysis. *Appl. Mech. Rev.* **2004**, *57*, 443–478. [CrossRef]
22. Berlioz, A.; Lamarque, C.-H. A non-linear model for the dynamics of an inclined cable. *J. Sound Vib.* **2005**, *279*, 619–639. [CrossRef]
23. Wang, J.J.; Zhu, S.J.; Liu, S.Y. Study on the mechanism for line spectrum reduction in nonlinear vibration isolation system. In Proceedings of the ASME International Design Engineering Technical Conferences & Computers and Information in Engineering, Las Vegas, NV, USA, 4–7 September 2007; pp. 1349–1354.
24. Kovacic, I.; Brennan, M.J.; Lineton, B. On the resonance response of an asymmetric Duffing oscillator. *Int. J. Non-Linear Mech.* **2008**, *43*, 858–867. [CrossRef]
25. Macdonald, J.H.G.; Dietz, M.S.; Neild, S.A.; Gonzalez-Buelga, A.; Crewe, A.J.; Wagg, D.J. Generalised modal stability of inclined cables subjected to support excitations. *J. Sound Vib.* **2010**, *329*, 4515–4533. [CrossRef]
26. Dankowicz, H.; Lacarbonara, W. On various representations of higher order approximations of the free oscillatory response of nonlinear dynamical systems. *J. Sound Vib.* **2011**, *330*, 3410–3423. [CrossRef]
27. Vassilopoulou, I.; Gantes, C.J. Nonlinear dynamic phenomena in a SDOF model of cable net. *Ingenieur-Archiv* **2012**, *82*, 1689–1703. [CrossRef]
28. Dai, H.-H.; Yue, X.-K.; Yuan, J.-P. A time domain collocation method for obtaining the third superharmonic solutions to the Duffing oscillator. *Nonlinear Dyn.* **2013**, *73*, 593–609. [CrossRef]
29. Huang, X.; Liu, X.; Sun, J.; Zhang, Z.; Hua, H. Vibration isolation characteristics of a nonlinear isolator using Euler buckled beam as negative stiffness corrector: A theoretical and experimental study. *J. Sound Vib.* **2014**, *333*, 1132–1148. [CrossRef]
30. Ozcelik, O.; Attar, P.J. Nonlinear response of flapping beams to resonant excitations under nonlinear damping. *Acta Mech.* **2015**, *226*, 4281–4307. [CrossRef]
31. Sari, M.S. Superharmonic resonance analysis of nonlocal nano beam subjected to axial thermal and magnetic forces and resting on a nonlinear elastic foundation. *Microsyst. Technol.* **2017**, *23*, 3319–3330. [CrossRef]
32. Elliott, A.J.; Cammarano, A.; Neild, S.A.; Hill, T.L.; Wagg, D. Comparing the direct normal form and multiple scales methods through frequency detuning. *Nonlinear Dyn.* **2018**, *94*, 2919–2935. [CrossRef] [PubMed]
33. Zhao, Y.; Huang, C.; Chen, L. Nonlinear planar secondary resonance analyses of suspended cables with thermal effects. *J. Therm. Stress.* **2019**, *42*, 1–20. [CrossRef]

34. Kandil, A. Internal resonances among the first three modes of a hinged–hinged beam with cubic and quintic nonlinearities. *Int. J. Non-Linear Mech.* **2020**, *127*, 103592. [CrossRef]
35. Arena, A.; Lacarbonara, W. Piezoelectrically induced nonlinear resonances for dynamic morphing of lightweight panels. *J. Sound Vib.* **2021**, *498*, 115951. [CrossRef]
36. Kandil, A.; Hamed, Y.S.; Alsharif, A.M.; Awrejcewicz, J. 2D and 3D Visualizations of the Mass-Damper-Spring Model Dynamics Controlled by a Servo-Controlled Linear Actuator. *IEEE Access* **2021**, *9*, 153012–153026. [CrossRef]
37. Su, X.; Kang, H.; Guo, T. Modelling and energy transfer in the coupled nonlinear response of a 1:1 internally resonant cable system with a tuned mass damper. *Mech. Syst. Signal Process.* **2021**, *162*, 108058. [CrossRef]
38. Long, Y.; Kang, H. Analysis of 1:1 internal resonance of a CFRP cable with an external 1/3 subharmonic resonance. *Nonlinear Dyn.* **2022**, *107*, 3425–3441. [CrossRef]
39. Kloda, L.; Lenci, S.; Warminski, J.; Szmit, Z. Flexural–flexural internal resonances 3:1 in initially straight, extensible Timoshenko beams with an axial spring. *J. Sound Vib.* **2022**, *527*, 116809. [CrossRef]
40. Kandil, A.; Hamed, Y.S.; Abualnaja, K.M.; Awrejcewicz, J.; Bednarek, M. 1/3 Order Subharmonic Resonance Control of a Mass-Damper-Spring Model via Cubic-Position Negative-Velocity Feedback. *Symmetry* **2022**, *14*, 685. [CrossRef]
41. Guo, T.; Rega, G. Nonlinear mode localization in boundary–interior coupled structures by an asymptotic approach. *Int. J. Non-Linear Mech.* **2022**, *141*, 103929. [CrossRef]
42. Dalela, S.; Balaji, P.S.; Jena, D.P. Design of a metastructure for vibration isolation with quasi-zero-stiffness characteristics using bistable curved beam. *Nonlinear Dyn.* **2022**, 1–41. [CrossRef]
43. Nayfeh, A.; Mook, D. *Nonlinear Oscillations*; Wiley: New York, NY, USA, 1995.